NUMERICAL STUDY OF GAS FLUIDIZED BEDS WITH IMERSED TUBES

Alexandre M. S. Costa, amscosta@uem.br
Flávio C. Colman, fcolman2@uem.br
Carlos Campanholi, campanholi@hotmail.com
Paulo R. Paraíso, paulo@deq.uem.br
Luiz M M Jorge, lmmjorge@deq.uem.br
Universidade Estadual de Maringá Av. Colombo 5790, bloco 104 , Maringá, PR, 87020-900

Abstract. *A numerical study based on a gas-solid eulerian-eulerian two fluid model has been conducted to predict bed fluid dynamics in face of immersed bank of tubes. The modeling is carried out using the open-source code MFIX. The two dimensional circular tubes' geometry is effected using the cartesian cut-cell feature. The study is acquitted to investigate the geometric effect and main physical model parameters influence on the numerical results. The erosion model used is based on the monolayer energy dissipation model which assumes that the rate of available energy for erosion close to a surface is a constant fraction of the kinetic energy dissipation by the solids particles. Computations are performed at different pressure levels, particle diameters and tube bank geometry. The results are compared with experimental measured values for erosion, bubble frequency and bubble velocity. A comparison between the frequency results and the experiments show the frequency and mean values are underestimated. However, some similar drifts were identified, e.g., greater frequency for greater excess velocities and for the bed with tubes, and maxima of bubble velocity.*

Keywords*: fluidized bed, computational fluid dynamics, MFIX*

1. INTRODUCTION

Fluidized beds are widely used in combustion and chemical industries. The immersed tubes are usually used for enhancement of heat transfer or control of temperature in fluidized beds. By his turn, tubes subjected to the solid particle impact may suffer severe erosion wear. Many investigations have been devoted to erosion in tubes immersed in fluidized beds on the various influencing factors (cf. Lyczkowski and Bouillard, 2002). As pointed by Achim et al. (2002), the factors can be classified as particle characteristics, mechanical design and operating conditions.

Some previous experimental studies have focused on bubble and particle behaviors (Kobayashi et al., 2000, Ozawa et al., 2002), tube attrition, erosion or wastage (Bouillard and Lyczkowski, 1991; Lee and Wang, 1995; Fan et al., 1998; Wiman, 1994), heat transfer (Wong and Seville, 2006, Wiman and Almstedt, 1997) and gas flow regimes (Wang et. al, 2002).

Previous numerical studies were also performed using different CFD codes. Recently He et al. (2009, 2004), using the K-FIX code adapted to body fitted coordinates investigated the hydrodynamics of bubbling fluidized beds with one to four immersed tubes. The erosion rates predicted using the monolayer kinetic energy dissipation model were compared against the experimental values of Wiman (1994) for the two tube arrangement. The numerical values were three magnitudes lower than the experimental ones. Also employing a eulerian-eulerian model and the GEMINI numerical code, Gustavsson and Almstedt (2000, 1999) performed numerical computations and comparison against experimental results (Enwald et. al., 1999). As reported for those authors, fairly good qualitative agreement between the experimental and numerical erosion results were obtained, and the contributions to the erosion from the different fluid dynamics phenomena near the tube were identified.

In the present study, is revisited the phenomena of the imersed tubes in a gas fluidized bed with three imersed tube arrangement employing the eulerian-eulerian two fluid model and the MFIX code. The purpose of the numerical simulations are to compare and explore some effects not previously investigated in the above mentioned references.

2. TWO FLUID AND EROSION MODELS

The mathematical model is based on the assumption that the phases can be mathematically described as interpenetrating continua; the point variables are averaged over a region that is large compared with the particle spacing but much smaller than the flow domain (see Anderson, 1967). A short summary of the equations solved by the numerical code in this study are presented next. Refer to Benyahia et al. (2006) and Syamlal et al. (1993) for more detailment.

The continuity equations for the fluid and solid phase are given by :

$$\frac{\partial}{\partial t}\left(\varepsilon_f \rho_f\right) + \nabla \bullet \left(\varepsilon_f \rho_f \vec{v}_f\right) = 0 \tag{1}$$

$$\frac{\partial}{\partial t}\left(\varepsilon_s \rho_s\right) + \nabla\bullet\left(\varepsilon_s \rho_s \vec{v}_s\right) = 0 \tag{2}$$

In the previous equations ε_f, ε_s, ρ_f, ρ_s, $\vec{v}_f$ and $\vec{v}_s$ are the volumetric fraction, density and velocity field for the fluid and solids phases..

The momentum equations for the fluid and solid phases are given by:

$$\frac{\partial}{\partial t}\left(\varepsilon_f \rho_f \vec{v}_f\right) + \nabla\bullet\left(\varepsilon_f \rho_f \vec{v}_f \vec{v}_f\right) = \nabla\bullet\bar{\bar{S}}_f + \varepsilon_f \rho_f \vec{g} - \vec{I}_{fs} \tag{3}$$

$$\frac{\partial}{\partial t}\left(\varepsilon_s \rho_s \vec{v}_s\right) + \nabla\bullet\left(\varepsilon_s \rho_s \vec{v}_s \vec{v}_s\right) = \nabla\bullet\bar{\bar{S}}_s + \varepsilon_s \rho_s \vec{g} + \vec{I}_{fs} \tag{4}$$

$\bar{\bar{S}}_f$ $\bar{\bar{S}}_s$ are the stress tensors for the fluid and solid phase. It is assumed newtonian behavior for the fluid and solid phases, i.e.,

$$\bar{\bar{S}} = \left(-P + \lambda\, \nabla\bullet\vec{v}\right)\bar{\bar{I}} + 2\mu\, S_{ij} \equiv -p\,\bar{\bar{I}} + \bar{\bar{\tau}} \qquad S_{ij} = \frac{1}{2}\left[\nabla\vec{v} + \left(\nabla\vec{v}\right)^T\right] - \frac{1}{3}\nabla\bullet\vec{v} \tag{5}$$

In the above equation P, λ, μ are the pressure, bulk and dynamic viscosity, respectively.

In addition, the solid phase behavior is divided between a plastic regime (also named as slow shearing frictional regime) and a viscous regime (also named as rapidly shearing regime). The constitutive relations for the plastic regime are related to the soil mechanics theory. Here they are representated as :

$$p_s^p = f_1\left(\varepsilon^*, \varepsilon_f\right) \qquad \mu_s^p = f_2\left(\varepsilon^*, \varepsilon_f, \phi\right) \tag{6}$$

In the above equation ε^* is the packed bed void fraction and ϕ is the angle of internal friction.

A detailing of functions f_1 to f_4 and f_9 can be obtained in Benyahia (2008).

On the other hand, the viscous regime behavior for the solid phase is ruled by two gas kinetic theory related parameters (e, Θ).

$$p_s^v = f_3\left(\varepsilon_s, \rho_s, d_p, \Theta, e\right) \qquad \mu_s^v = f_4\left(\varepsilon_s, \rho_s, d_p, \Theta^{1/2}, e\right) \tag{7}$$

The solid stress model outlined by Eqs. (6) and (7) will be quoted here as the standard model. Additionally, a general formulation for the solids phase stress tensor that admits a transition between the two regimes is given by :

$$\bar{\bar{S}}_s = \begin{cases} \phi\left(\varepsilon_f\right)\bar{\bar{S}}_s^v + \left[1-\phi\left(\varepsilon_f\right)\right]\bar{\bar{S}}_s^p & \text{if } \varepsilon_f < \varepsilon^* + \delta \\ \bar{\bar{S}}_s^v & \text{if } \varepsilon_f \geq \varepsilon^* + \delta \end{cases} \tag{8}$$

According to Pannala et al.(2009), two diferent formulations for the weighting parameter "ϕ" can be employed :

$$\phi(\varepsilon) = \frac{1}{1+\upsilon^{\frac{\varepsilon-\varepsilon^*}{2\delta\varepsilon^*}}} \qquad \phi(\varepsilon) = \frac{\mathrm{Tanh}\left(\frac{\pi\left(\varepsilon-\varepsilon^*\right)}{\delta\varepsilon^*}\right)+1}{2} \tag{9}$$

In the above equation the void fraction range δ and the shape factor υ are smaller values less than unity. It must be emphasized that when δ goes to zero and ϕ equals to unity, the "switch" model as proposed by Syamlal et al. (1993) based on the Schaeffer (1987) can be recovered.

On the other hand, the Srivastava and Sundaresan (2003), also called "Princeton model", can be placed on the basis of Eq. (9)

Also in equations (4) and (5) $\vec{I}_{fs}$ is the momentum interaction term between the solid and fluid phases, given by

$$\vec{I}_{fs} = -\varepsilon_s \nabla P_f - \beta\left(\vec{v}_s - \vec{v}_f\right) \tag{10}$$

There is a number of correlations for the drag coefficient β (Eqs. 11 to 16). The first of the correlations for the drag coefficient is based on Wen and Yu (1966) work. The Gidaspow drag coefficient is a combination between the Wen Yu correlation and the correlation from Ergun (1952). The Gidaspow blended drag correlation allows controlling the transition from the Wen and Yu, and Ergun based correlations. In this correlation the χ blending function was originally

proposed by Lathowers and Bellan (2000) and the value of parameter *C* controls the degree of transition. From Eq. (14), the correlation proposed by Syamlal and O'Brien (1993) carries the advantage of adjustable parameters C_1 and d_1 for different minimum fluidization conditions. The correlations given in Eq. (15) and Eq. (16) are based on Lattice-Boltzmann simulations. For detailments of these last drag correlations refer to the works by Benyahia et al. (2006) and Wang et al. (2010).

$$\beta_{\text{Wen-Yu}} = \frac{3}{4} C_D \frac{\rho_f \varepsilon_f \varepsilon_s \left|\vec{v}_f - \vec{v}_s\right|}{d_p} \varepsilon_f^{-2.65} \qquad C_D = \begin{cases} \dfrac{24}{\text{Re}}\left(1 + 0.15\,\text{Re}^{0.687}\right) & \text{Re}<1000 \\ 0.44 & \text{Re} \geq 1000 \end{cases} \qquad \text{Re} = \frac{\rho_f \varepsilon_f \left|\vec{v}_f - \vec{v}_s\right| d_p}{\mu_f} \tag{11}$$

$$\beta_{\text{Gidaspow}} = \begin{cases} \beta_{\text{Wen-Yu}} & \varepsilon_f > 0.8 \\ \beta_{\text{Ergun}} = \dfrac{150\,\varepsilon_s (1-\varepsilon_s)\mu_f}{\varepsilon_f d_p^2} + \dfrac{1.75\,\rho_f \varepsilon_s \left|\vec{v}_f - \vec{v}_s\right|}{d_p} & \varepsilon_f \leq 0.8 \end{cases} \tag{12}$$

$$\beta_{\text{Gidaspow-blended}} = \chi\,\beta_{\text{Wen-Yu}} + (1-\chi)\beta_{\text{Ergun}} \qquad \chi = \frac{\tan^{-1}\left(C\,(\varepsilon_f - 0.8)\right)}{\pi} + 0.5 \tag{13}$$

$$\beta_{\text{Syamlal-OBrien}} = \frac{3}{4} \frac{\rho_f \varepsilon_f \varepsilon_s}{V_r^2 d_p} \left(0.63 + 4.8\sqrt{\frac{V_r}{\text{Re}}}\right)^2 \left|\vec{v}_f - \vec{v}_s\right|$$

$$V_r = 0.5A - 0.03\,\text{Re} + 0.5 \times \sqrt{(0.06\,\text{Re})^2 + 0.12\,\text{Re}\,(2B - A) + A^2} \tag{14}$$

$$A = \varepsilon_f^{4.14} \qquad B = \begin{cases} C_1 \varepsilon_f^{1.28} & \varepsilon_f \leq 0.85 \\ \varepsilon_f^{d_1} & \varepsilon_f > 0.85 \end{cases}$$

$$\beta_{\text{Hill-Koch-Ladd}} = 18\mu_f (1-\varepsilon_s)^2 \varepsilon_s \frac{F}{d_p^2} \qquad F = f_9\left(F_0, F_1, F_2, F_3\right) \tag{15}$$

$$\beta_{\text{Beestra}} = 180\frac{\mu_f \varepsilon_s^2}{d_p^2} + 18\frac{\mu_f \varepsilon_f^3 \varepsilon_s \left(1 + 1.5\sqrt{\varepsilon_s}\right)}{d_p^2} + 0.31\frac{\mu_f \varepsilon_s\,\text{Re}}{\varepsilon_f d_p^2} \frac{\left[\varepsilon_f^{-1} + 3\varepsilon_f \varepsilon_s + 8.4\,\text{Re}^{-0.343}\right]}{\left[1 + 10^{3\varepsilon_s}\,\text{Re}^{-0.5-2\varepsilon_s}\right.} \tag{16}$$

For closing the model, a transport equation for the granular energy Θ provides a way of determine the pressure and viscosity for the solid phase during the viscous regime. Equation (5) is a transport equation for the granular energy Θ. Its solution provides a way of determine the pressure and viscosity for the solid phase during the viscous regime. The terms κ_s γ and ϕ_{gs} are the granular energy conductivity, dissipation and exchange, respectively.

$$\frac{3}{2}\left[\frac{\partial}{\partial t}\varepsilon_s \rho_s \Theta + \nabla \bullet \rho_s \vec{v}_s \Theta\right] = \overline{\overline{S}}_s : \nabla \vec{v}_s - \nabla \bullet \left(\kappa_s \nabla \Theta\right) - \gamma + \phi_{gs} \tag{17}$$

$$\kappa_s = f_5\left(\varepsilon_s, \rho_s, d_p, \Theta^{1/2}, e, \beta\right) \qquad \gamma = f_6\left(\varepsilon_s, \rho_s, d_p, \Theta^{3/2}, e\right) \qquad \phi_{gs} = f_7\left(\varepsilon_s, \rho_s, d_p, \Theta, \left|\vec{v}_f - \vec{v}_s\right|, \beta\right) \tag{18}$$

In the algebraic approach, instead solving the full equation (6) , the granular energy is obtained by equating the first term on the right hand side with the dissipation term.

The model where Eqs. (5) to (8) and (17) are solved is the kinetic theory model, termed here as KTGF. Conversely, in the constant solids viscosity model (CVM) the solids pressure is defined as in Eq. (6) and the solids viscosity in either plastic and viscous regimes is set constant.

For erosion calculations in this work the monolayer energy dissipation model (Lyczkowski and Bouillard, 2002) is used. In that model the kinetic energy dissipation rate for the solids phase in the vicinity of stationary immersed surfaces is related to erosion rate in m/s by multiplication with an appropriate constant. This constant is function of surface hardness, elasticity of collision and diameter of particles hitting the surface. The kinetic energy dissipation rate Φ_s in W/m^3 for the solids phase is given by :

$$\Phi_s = \left[\varepsilon_s \overline{\overline{\tau}}_s : \nabla \vec{v}_s + \beta \frac{\vec{v}_s^{\,2}}{2} \right] \tag{19}$$

4. NUMERICAL METHOD

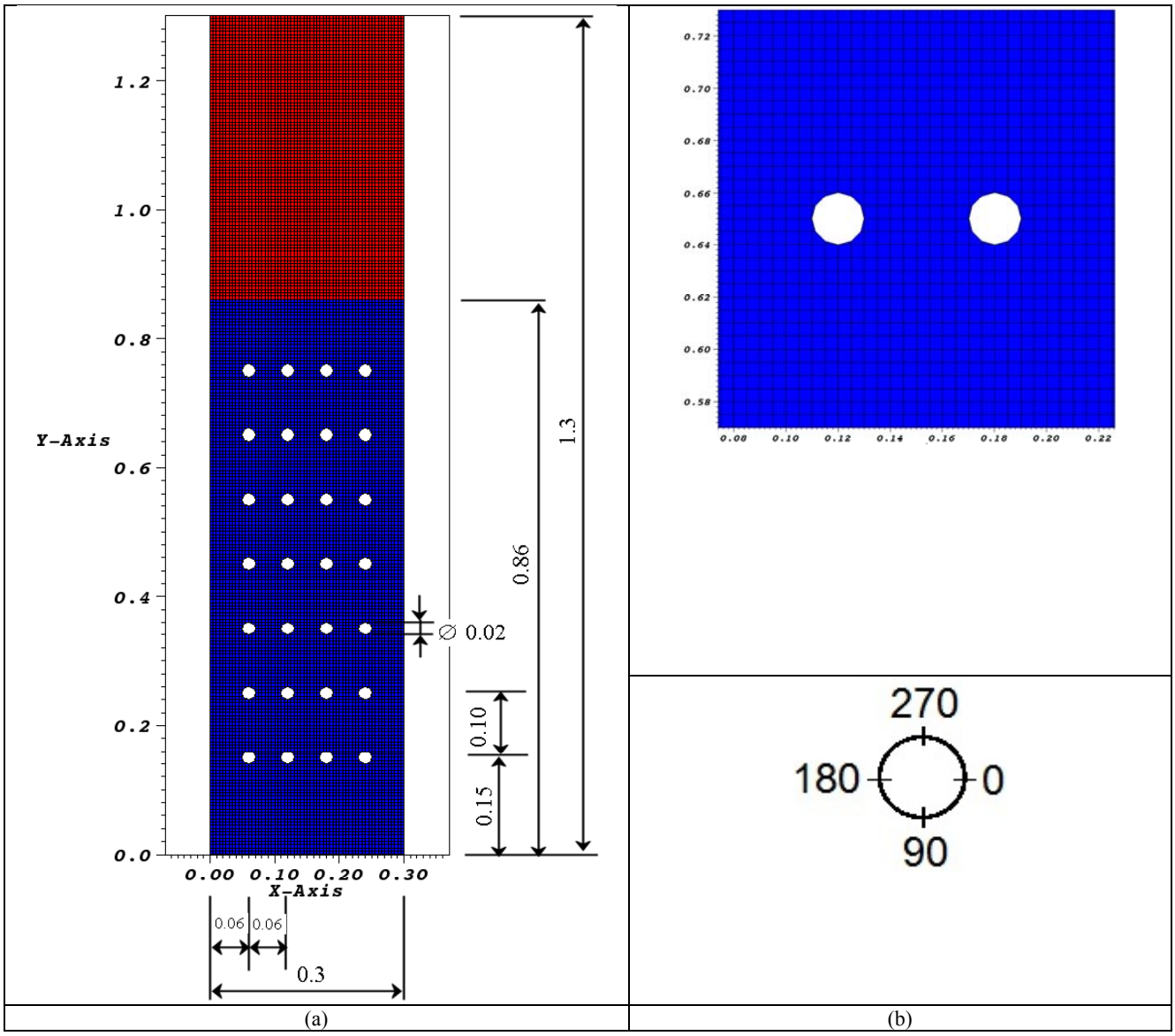

Figure 1. (a) I4 arrangement mesh and (b) detailment around an obstacle

Figure 1 above portrays the domain for the numerical simulations and four circumferential angles references for erosion measurement. The code MFIX (Multiphase Flow with Interphase eXchanges) is an open source CFD code developed at the National Energy Technology Laboratory (NETL) for describing the hydrodynamics, heat transfer and chemical reactions in fluid-solids systems. It has been used for describing bubbling and circulating fluidized beds, spouted beds and gasifiers. MFIX calculations give transient data on the three-dimensional distribution of pressure, velocity, temperature, and species mass fractions.

The hydrodynamic model is solved using the finite volume approach with discretization on a staggered grid. A second order accurate discretization scheme was used and superbee scheme was adopted for discretization of the convective fluxes at cell faces for all equations in this work. With the governing equations discretized, a sequential iterative solver is used to calculate the field variables at each time step. The main numerical algorithm is an extension of SIMPLE. Modifications to this algorithm in MFIX include a partial elimination algorithm to reduce the strong coupling between the two phases due to the interphase transfer terms. Also, MFIX makes use of a solids volume fraction correction step instead of a solids pressure correction step which is thought to assist convergence in loosely packed

regions. Finally, an adaptive time step is used to minimize computation time. See Syamlal (1998) for more details. The immersed obstacles were implemented using the cut-cell technique available in the code (Dietiker, 2009)

The numerical runs were based on experiments of Wiman (1994, 1997) in an air pressurized bed with horizontal tubes for three different tube-bank geometries. The S4 and S4D tubes geometry are given in Figure 2.The cartesian two-dimensional grid employed after mesh refinement is outlined in Figure 1b. The mesh employed for the bed without tube, and the I4 arrangement was 60 × 260 cells, and for the S4 and S4D arrangement 60 × 340. The bed was operated at room temperature (24 C) at pressures between 0.1 and 1.6 MPa and at two different excess velocities: $U_{fl} - U_{mf} = 0.2$ m/s and $U_{fl} - U_{mf} = 0.6$ m/s. Here, U_{fl} is the superficial fluidization velocity based on the free bed cross-section. The voidage at minimum fluidization was 0.46 and the minimum fluidization velocities was 0.42 , 0.31 and 0.18 m/s, for 0.1, 0.4 and 1.6 MPa pressures, correspondingly. The particle diameter and density were 700 μm and 2600 kg/m^3. The bubble parameters obtained from simulation were based on methodology described in Almstedt (1987), using numerical probes in the domain, centered at (0.15, 0.55) and separated from 15 mm. The target tube for erosion measurements is the one centered at (0.18, 0.55) for all the tube arrangements. More information about the experiments can be accessed from Wiman (1994, 1997).

In this work, the parameters for controlling the numerical solution (e.g., under-relaxation, sweep direction, linear equation solvers, number of iterations, residual tolerances) were kept as their default code values. Moreover, for setting up the mathematical model, when not otherwise specified the code default values were used. The computer used in the numerical simulations was a PC with OpenSuse linux and Intel Quad Core processor. The simulation time was 20 s.

For generating the numerical results, the parameters listed above, referred here as baseline simulation, were employed. In addition, for the baseline simulation were employed the Syamlal-O´Brien drag model, the standard solid stress model, and slip and non-slip condition for solid and gas phase, correspondingly. The previous set of models will be referred in the result's section as baseline simulation models.

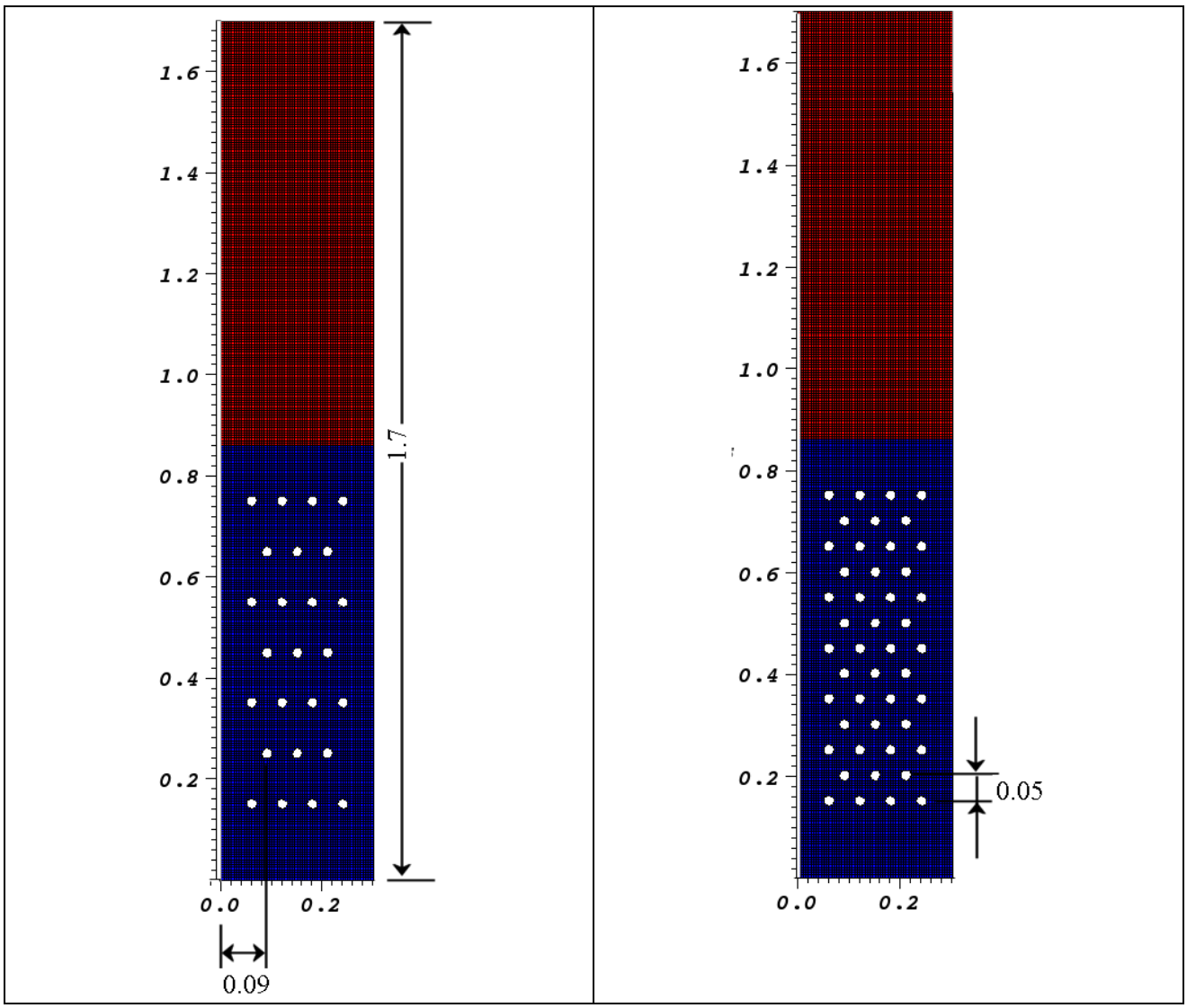

(a)	(b)

Figure 2. Mesh for (a) S4 and (b) S4D tube arrangement

5. RESULTS AND DISCUSSION

Figure 3 is a sampling plot showing the instantaneous gas volumetric fraction fields for different tube arrangements. Analysis of Fig. (3) shows the influence of immersed obstacles on the bubble splitting mechanism taking place and the bubble passage pattern. Above the tube bank, the bubble appears to grow to size similar to the without tube geometry. For the geometry with tubes the bubble encompasses the obstacles but not at the full width of the bed. The interaction is stronger for the denser tube geometry.

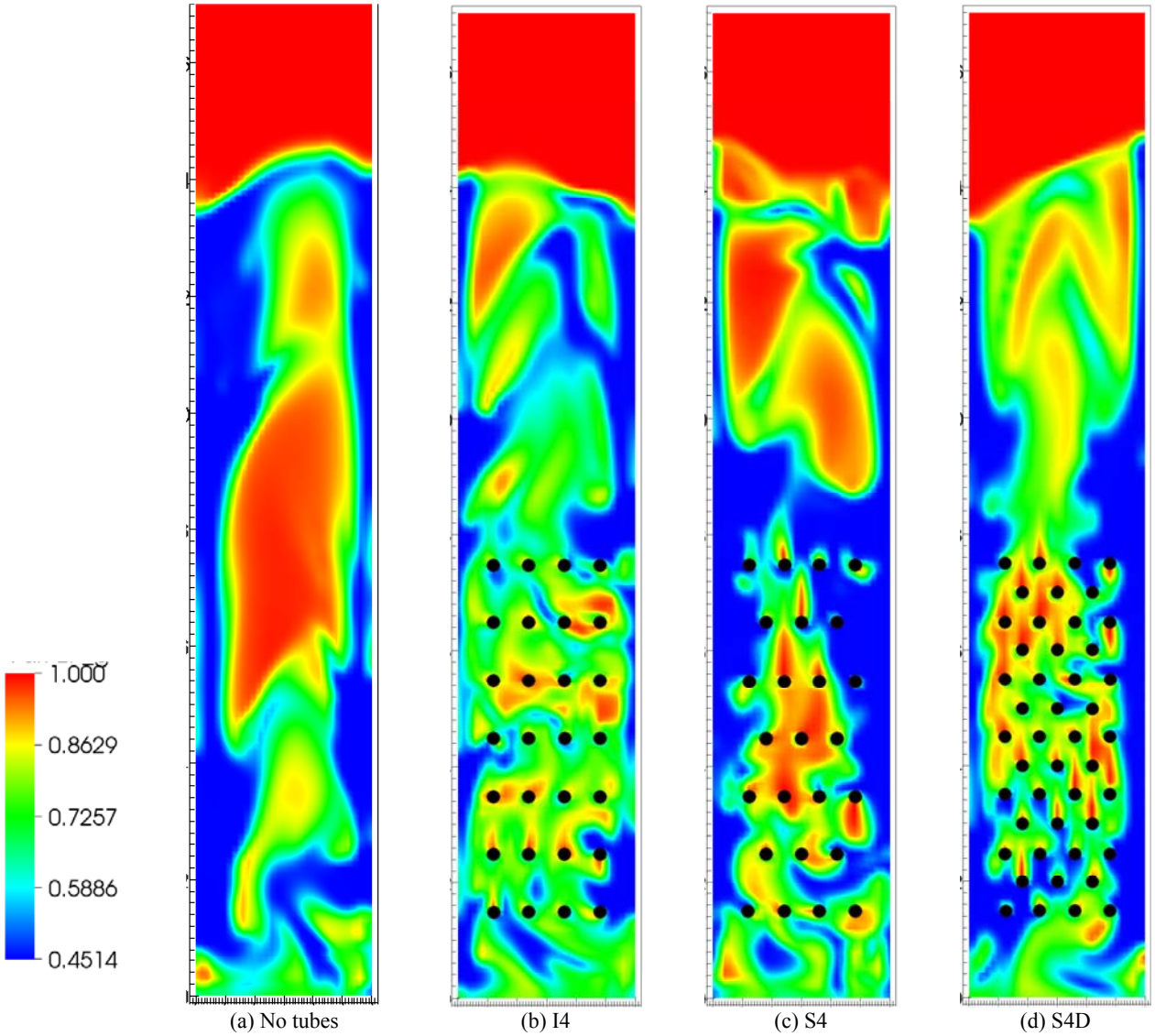

Figure 3. Snapshots of voidage field at 4 s for different tube arrangements. P = 0.4 MPa , Uf = 0.6 m/s

Figure 4 shows a comparison between the numerically predicted values of bubble frequency, using the baseline simulation models discussed in section 4, and those based on the experimental measurements from the works of Almstedt (1987) and Wiman (1995). As shown in the Fig. 4, the calculated values of N_b are underestimated at higher pressures, while at low pressures, there is a quite good agreement between calculated and experimental results. This conclusion holds true both for the I4 and for the S4D tube arrangement. As in the experimental results there are no noticeable differences for the two tubes arrangements.

Figure 5 shows a comparison for the bubble frequency for the bed without tube and with the S4 arrangement. As shown in Fig. 5(a) for the bed without tubes the trend points to a frequency agreement between 0.4 and 0.6 MPa. Up this range the values differences increases as pressures increases up to 1.6 MPa. For the S4 arrangement the trend is similar

to the I4 and S4D arrangement. The experimental results depicted in Figs. 4 and 5 suggest that the frequency increases with pressure both with and without tubes. For numerical results this holds true only for low pressures, i.e., 0.1 and 0.4 MPa. The numerical results suggest a maxima occurring between 0.4 and 1.6 MPa. On the other hand, the numerical results corroborate the experimental trend that the mean frequency is higher for the bed with tubes than for the freely bubbling bed.

Figure 6 and 7 shows a comparison for the mean bubble velocity Vb. In all cases, the simulated results are underestimated in relation to the experiments. However, the trend observed for the experimental results with a maxima around 0.4 MPa is verified for the numerical results for all the tube arrangements. For the bed without tubes the experimental increase trend of Vb with pressure is valid for pressures higher than 0.4 MPa.

Figure 8 shows a comparison for the bubble frequency for $U_f = 0.2$ m/s. Comparison with results in Fig. 4 shows that the numerical results, although smaller are closer to the experimental. The tendency holds true for both S4 and S4D arrangements. Comparison with the numerical results for the S4D and S4 arrangements given in Fig. 4 and 5, also shows that Nb increases with increasing excess velocity. The last, is the same drift verified for the experimental values.

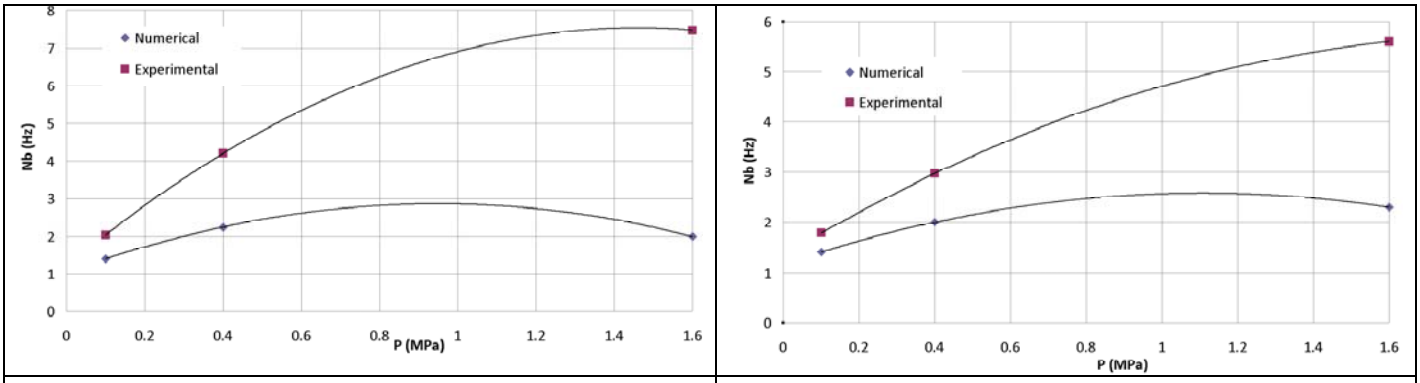

I4 0_6Uf | S4D 0_6Uf

Figure 4. Nb versus pressure, numerical X experimental

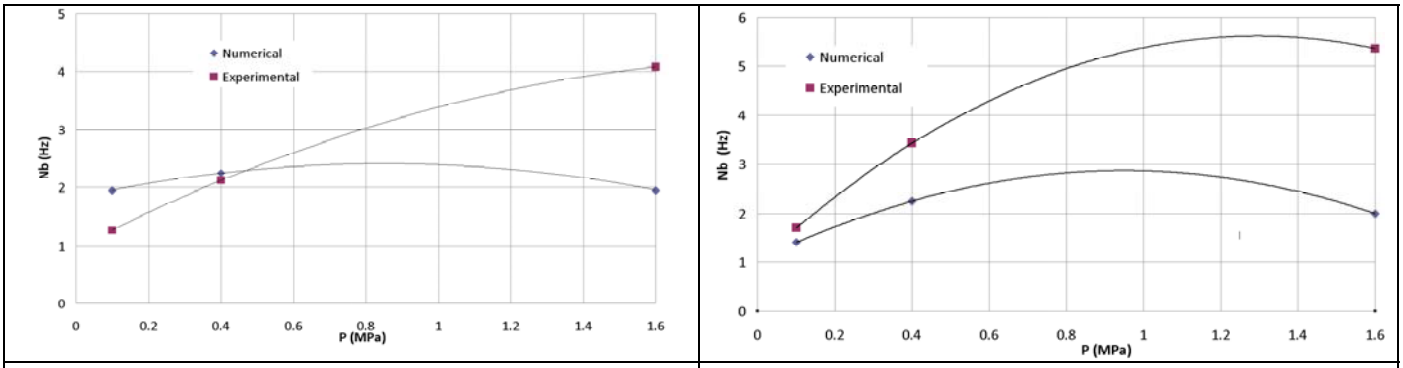

NO TUBE 0_6Uf | S4 0_6Uf

Figure 5. Nb versus pressure, numerical X experimental

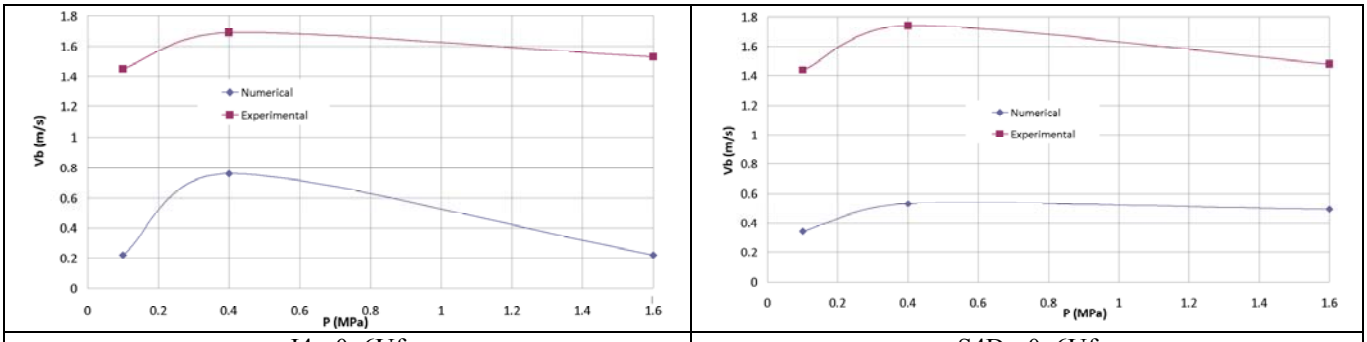

I4 - 0_6Uf | S4D - 0_6Uf

Figure 6. Vb versus pressure, numerical X experimental

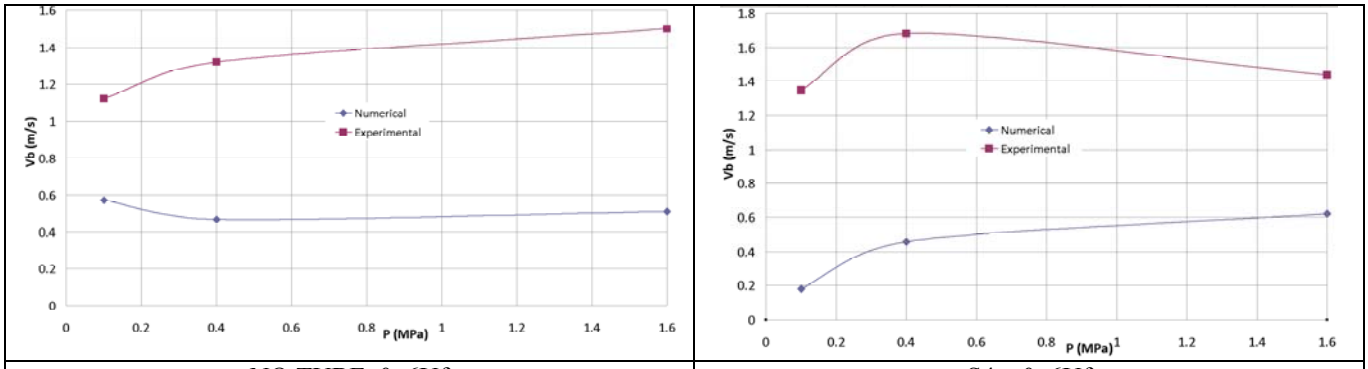

NO TUBE 0_6Uf | S4 – 0_6Uf

Figure 7. Vb versus pressure, numerical X experimental

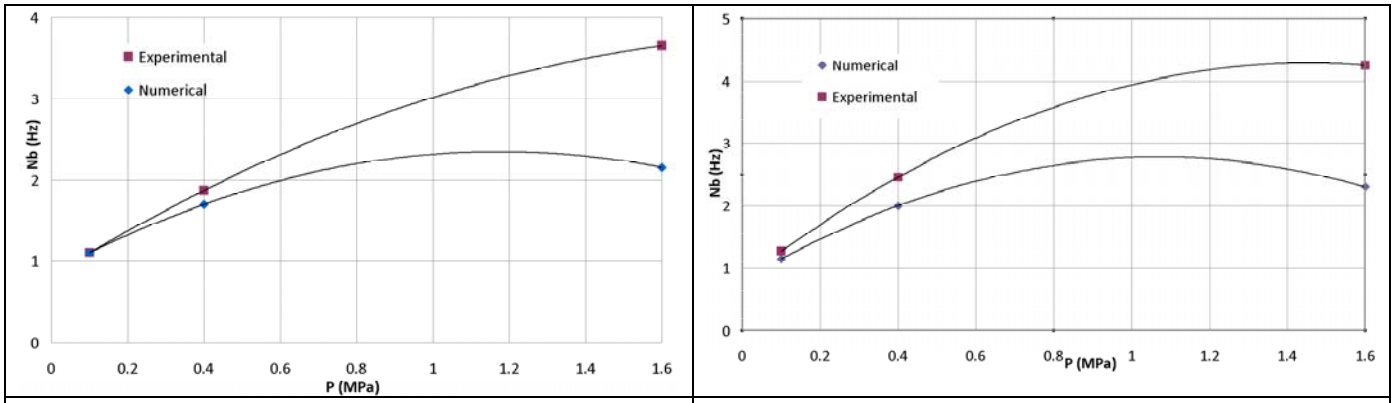

S4_0_2Uf | S4D_0_2Uf

Figure 8. Nb versus pressure, numerical X experimental

Figure 9 presents the tendency lines for the time averaged kinetic energy dissipation as a function of circumferential position θ on the tube surface for the S4 arrangement for two distinct pressures. As it would be seen the highest experimental results are between 90 and 240 degrees, while for the numerical are between 30 and 150. The numerical values are over predicted in the range 0 to 100 degrees and above 240 degrees. In the range from 100 to 240 degrees the numerical are below the experimental. Similar trends are verified for the 1.6 MPa pressure, with the experimental curves less sensitive to pressure variation . By his turn the numerical values, show more sensitivity to pressure, although with the same magnitude order.

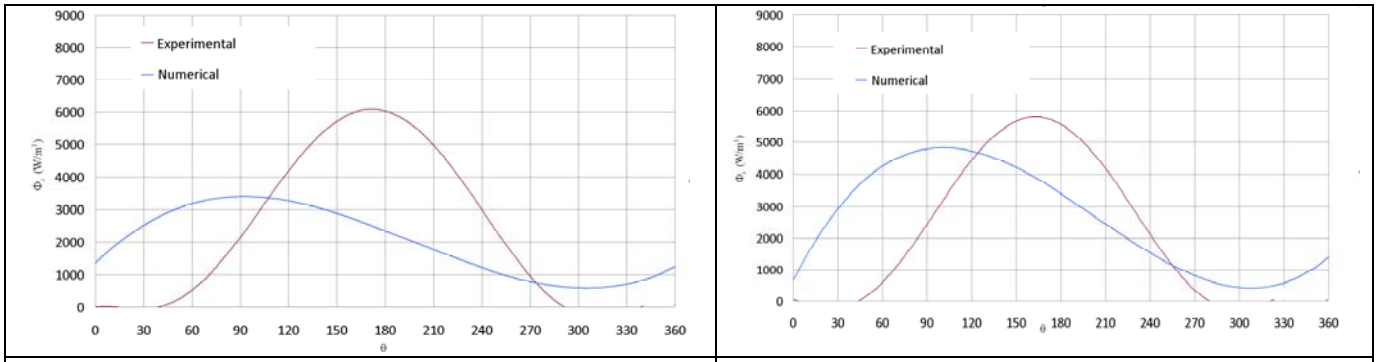

S4 – 0_1MPa | S4- 1_6MPa

Figure 9. Time averaged kinetic energy dissipation predicted for different tube arrangements at two different operating pressures.

6. CONCLUSIONS

In this work was investigated numerically the hydrodynamics of a two dimensional bed with immersed tubes. The simulations were based on an experimental bed with different tube bank geometries, operating pressures and gas

excess velocities. The objective of this study was two fold: explore and investigate some effects not previously explored in the literature, to verify the feasibility of the MFIX code for such a kind of study. The simulation's results were framed in terms of bubble parameters (frequency and mean velocity) and solids kinetic energy dissipation. A comparison between the frequency results and the experiments show the frequency and mean values are underestimated. However, some similar drifts were identified, e.g., greater frequency for greater excess velocities and for the bed with tubes, and maxima of bubble velocity. At this point, some factors that possibly improve our bubble parameters results can be enlisted, bubble distribution and movement around the bed center, solid stress model setting, drag correlation. By his turn, for the solids kinetic dissipation energy, the range of angles that gives maximum values are shifted in relation to the experiments. Finally, remarks towards better agreement with experimental values can also be done for the energy dissipation model. Specifically, according to the monolayer erosion model and its discussion above Eq. (19) some degree of uncertainty is associated to the multiplying constant, as the exact value of elasticity of collision is not known.

7. REFERENCES

Achim, D., Easton, A. K., Schwarz, M. P., Witt, P.J., Zakhari, A., 2002, "Tube erosion modelling in a fluidised bed", Applied Mathematical Modelling, Vol 26, pp. 191-201.

Almstedt, A. E., 1987, A study of bubble behaviour and gas distribution in pressurized fluidized beds burning coal. Thesis for the degree of Licentiate of Engineering, Chalmers University of Technology, Goteborg. Sweden.

Anderson, T. B., 1967, "A fluid mechanical description of fluidized beds: Equations of motion", Industrial Engineering Chemical Fundamentals, Vol 6, pp. 527-539.

Benyahia, S., 2008, "Validation study of two continuum granular frictional flow theories", Industrial Engineering Chemical Research, 47, 8926-8932.

Benyahia, S., Syamlal, M., O'Brien, T. J., "Summary of MFIX Equations 2005-4", 1 March 2006: <http://www.mfix.org/documentation/MfixEquations2005-4-1.pdf>.

Benyahia, S., Syamlal, M., O'Brien, T. J., 2006, "Extension of Hill–Koch–Ladd drag correlation over all ranges of Reynolds number and solids volume fraction", Powder Technology, 162, 166-174.

Bouillard, J. X., Lyczkowski, R. W., 1991, "On the erosion of heat exchanger tube banks in fluidized-bed combustor", Powder Technology, Vol 68, pp. 37-51.

Dietiker, J., "Cartesian Grid User Guide", 4 September 2009: <https://mfix.netl.doe.gov/documentation/Cartesian_grid_user_guide.pdf>.

Enwald, H., Peirano, E., Almstedt, A. E., Leckner, B., 1999, "Simulation of the fluid dynamics of a bubbling fluidized bed: Experimental validation of the two-fluid model and evaluation of a parallel multiblock solver", Chemical Engineering Science, 54, 311-328.

Ergun, S., 1952, "Fluid-flow through packed columns", Chemical Engineering Progress, Vol 48, n. 2, pp. 91-94.

Fan, J. R., Sun, P., Chen, L. H., Cen, K. F., 1998, "Numerical investigation of a new protection method of the tube erosion by particle impingement", Wear, Vol 223, pp. 50-57.

Gustavsson, M., Almstedt, A. E., 1999, "Numerical simulation of fluid dynamics in fluidized beds with horizontal heat exchanger tubes", Chemical Engineering Science, 55, 857-866.

Gustavsson, M., Almstedt, A. E., 2000, "Two-fluid modelling of cooling-tube erosion in a fluidized bed", Chemical Engineering Science, 55, 867-879.

He, Y. R., Lu, H. L., Sun, Q. Q., Yang, L. D., Zhao, Y. H., Gidaspow, D., Bouillard, J., 2004, "Hydrodynamics of gas-solid flow around immersed tubes in bubbling fluidized beds", Powder Technology, 145, pp. 88-105.

He, Y. R., Zhan, W., Zhao, Y., Lu, H. Schlaberg, I., 2009, "Prediction on immersed tubes erosion using two-fluid model in a bubbling fluidized bed", Chemical Engineering Science, 64, pp. 3072-3082.

Kobayashi, N., Yamazaki, R., Mori, S., 2000, "A study on the behaviour of bubbles and solids in bubbling fluidized beds", Powder Technology, Vol 113, pp. 327-344.

Lathowers, D., Bellan, J., 2000, "Modeling of dense gas-solid reactive mixtures applied to biomass pyrolysis in a fluidized bed", Proceedings of the 2000 U.S. DOE Hydrogen Program Review, NREL/CP-570-28890. USA.

Lee, S. W., Wang, B. Q., 1995, "Effect of particle-tube collision frequency on material wastage on in-bed tubes in the bubbling fluidized bed combustor", Wear, Vol 184, pp. 223-229.

Lyczkowski, R. W., Bouillard, J. X., 2002, "State-of-the-art review of erosion modeling in fluid/solid systems", Progress in Energy and Combustion Science, Vol 28, pp. 543-602.

Ozawa, M., Umekawa, H., Furui, S., Hayashi, K., Takenaka, N., 2002, "Bubble behavior and void fraction fluctuation in vertical tube banks immersed in a gas-solid fluidized-bed model", Experimental Thermal and Fluid Science, Vol 26, pp. 643-652.

Pannala, S., Daw, C. S., Finney, C. E. A., Benyahia, S., Syamlal, M., O´Brien, T. J., "Modelling the collisional-plastic stress transition for bin discharge of granular material", 2009, Powders and Grains 2009 – Proceeding of the 6th International Conference on Micromechanics of Granular Media, pp. 657-660.

Schaeffer, D. G., 1987, "Instability in the evolution equations describing incompressible granular flow", Journal Differential Equations, v. 66, pp. 19-50.

Siravastava, A., Sundaresan, S., 2003, "Analysis of a frictional–kinetic model for gas–particle flow", Powder Technology, v. 129, pp. 72-85.

Syamlal, M., 1998, "MFIX Documentation, Numerical Techniques", Technical Note, DOE/MC-31346-5824, NTIS/DE98002029, National Technical Information Service, Springfield, VA, USA.

Syamlal, M., Rogers, W. A., O'Brien, T. J., 1993, "MFIX Documentation, Theory Guide", Technical Note, DOE/METC-94/1004, NTIS/DE94000087, National Technical Information Service, Springfield, VA, USA.

Wang, J., van der Hoef, M. A., Kuipers, J. A. M., 2010,"CFD study of the minimum bubbling velocity of Geldart A particles in gas-fluidized beds", Chemical Engineering Science, 65, pp. 3772-3785.

Wen, C. Y., Yu, Y. H., 1966, "Mechanics of Fluidization", Chemical Engineering Progress Symposium Series, Vol 62, n. 62, pp. 100-111.

Wiman, J., 1994, An experimental study of hydrodynamics and tube erosion in a pressurized fluidized with horizontal tubes. Thesis for the degree of Licentiate of Engineering, Chalmers University of Technology, Goteborg. Sweden.

Wiman, J., Almstedt, A. E., 1997, "Hydrodynamics, erosion and heat transfer in a pressurized fluidized bed: influence of pressure, fluidization velocity, particle size and tube bank geometry", Chemical Engineering Science, Vol 52, pp. 2677-2695.

Wong, Y. S., Seville, J. P. K., 2006, "Single-particle motion and heat transfer in fluidized beds", AIChe Journal, Vol 52, pp. 4099-4109.

5. RESPONSIBILITY NOTICE

The authors are the only responsible for the printed material included in this paper.